Progress in Natural Science: Materials International 2013;23(5):487–492

Chinese Materials Research Society

Progress in Natural Science: Materials International

www.elsevier.com/locate/pnsmi
www.sciencedirect.com

ORIGINAL RESEARCH

Induced modifications in the properties of Sr doped $BiFeO_3$ multiferroics

Tanvir Hussain[a,*], Saadat A. Siddiqi[a,b], Shahid Atiq[a], M.S. Awan[c]

[a]*Centre of Excellence in Solid State Physics, Quaid-e-Azam Campus, University of the Punjab, Lahore 54590, Pakistan*
[b]*Interdisciplinary Research Centre in Biomedical Materials (IRCBM), COMSATS Institute of Information Technology, Off Raiwind road, Lahore, Pakistan*
[c]*Department of Physics, COMSATS Institute of Information Technology, Islamabad, Pakistan*

Received 10 April 2013; accepted 27 June 2013
Available online 6 October 2013

KEYWORDS

Bismuth ferrite;
Ferroelectricity;
Ferromagnetism;
Nanomaterials;
Magnetically ordered materials

Abstract Multiferroics exhibit unique combination of ferroic properties, simultaneously. For instance, in $BiFeO_3$, magnetic and electric properties co-exist. In this work, $BiFeO_3$ and Sr-doped $BiFeO_3$ samples with general formula, $Bi_{1-x}Sr_xFeO_3$ ($x=0.00$, 0.05, 0.10, 0.20, and 0.30) were synthesized by sol–gel auto-combustion technique, in order to investigate these ferroic properties. The samples were confirmed to have perovskite type rhombohedral structure, characteristic of $BiFeO_3$. A dilute phase of $Bi_2Fe_4O_9$ was also found in all the Sr-doped samples. The micrographs of the palletized samples revealed that minutely doped Sr might not have any effect on the morphology of the samples. Frequency dependent dielectric measurements were carried out at room temperature for all the samples from 100 Hz to 1 MHz. The dielectric constant of un-doped sample at low frequency was 52 which decreased with increasing Sr doping. An enhancement of magnetic properties was observed with increasing the Sr contents. Pure $BiFeO_3$ material was observed to have the least value of remanent magnetization. As the Sr^{2+} ions were doped in $BiFeO_3$, its magnetization and remanence were increased to 0.867 emu/g and 0.175 emu/g, respectively, at $x=0.30$.

1. Introduction

In contrast to conventional electronic devices which utilize only the charge degree of freedom, spintronic devices take advantage of the electron spin degree of freedom and thus unite magnetic and electric properties. Owing to their application relevance and outstanding fundamental physical principles, they have been included among vigorously investigated research topics, in the recent past [1]. As far as their technological applications are

*Corresponding author.
E-mail address: tanvirhussainssp905@gmail.com (T. Hussain).

Peer review under responsibility of Chinese Materials Research Society.

ELSEVIER Production and hosting by Elsevier

1002-0071 © 2013 Chinese Materials Research Society. Production and hosting by Elsevier B.V. All rights reserved.
http://dx.doi.org/10.1016/j.pnsc.2013.09.004

concerned, spintronic devices are, nowadays, most prominently being used as hard disk drive reading heads. Controlling magnetization has been a very important aspect for the realization of spintronic devices. Naturally, the magnetization can be controlled by external magnetic fields. However, the implementation of magnetic fields of sufficient strength to switch the magnetization is technologically difficult on sufficiently small length scales and power consuming, as well. Hence, other approaches to control the magnetization are badly required. From a technological view point, electric fields are easy to implement on even very small length scales, power efficient and fully switchable. The ability to reversibly switch the magnetization orientation by an electric field is thus considered a milestone on the way to new functional spintronic devices [1,2]. The necessary physical properties for such an electrically controllable magnetization are expected to present in materials that exhibit ferromagnetic and ferroelectric properties at the same time. Thus, multiferroic materials are an important topic of current research as multiferroic devices may be employed in future random access memories that combine the advantages of magnetic and ferroelectric random access memories [3]. Mostly, multiferroic materials are divided in two major categories; type-I and type-II multiferroics. In the former, the origin of magnetism and ferroelectricity is in different materials and hence, the coupling of magnetic and ferroelectric subsystems in perovskites is rather weak. In later, electromagnetic coupling is very strong, as in this type, ferroelectricity is induced due to certain ordering of magnetic moments in the magnetic state. In type-I multiferroics, most of the materials have perovskite structure like ABO_3 (A and B are transition metals). In these materials, ferroelectricity is generated due to transition metal 'A' with d^o configuration whereas magnetism is produced by transition metal 'B' with d^n (n is the odd number of electrons) configuration [4]. In ABO_3 multiferroics, ferrroelectricity and electromagnetic coupling are very exciting; they are useful for practical applications at room temperature (RT) [5]. $BiFeO_3$ (BFO) is a type-I multiferroic material having rhombohedral perovskite structure. It is a very promising material due to application view point because it is the only RT multiferroic material. BFO has G-type antiferromagnetic structure in which each Fe^{3+} ion (responsible for effective magnetic moment) is surrounded by six Fe^{3+} nearest neighbors with antiparallel moments. G-type structure is a spiral arrangement of the magnetic moments of Fe^{3+} ions, and the canted spins arising from Dzyloshinsii–Moriya (DM) interaction cause slight deviation from ideal antiferromagnetic behavior giving rise to weak ferromagnetism in BFO [6,7]. In addition, BFO has a large polarization, high Curie ($T_c \sim 810$ °C) and Neel temperatures ($T_N \sim 380$ °C) [8].

Despite such favorable properties, technological applicability of BFO is restricted due to many reasons, for instance, formation of secondary phase, very weak magnetization and weak electromagnetic coupling. To improve the multiferroic characteristics of BFO, alkaline earth metals might be substituted. In this regard, Sr has been understood as an appropriate choice for substitution at Bi-site because the ionic radius of Sr^{2+} is 1.18 Å, comparable to Bi^{3+} (1.03 Å). This substitution would create a charge imbalance that could be compensated in three possible ways: (i) charge disproportion of Fe^{3+} and Fe^{5+}, (ii) partial conversion of Fe^{3+} to Fe^{4+} and (iii) creation of oxygen vacancies. All these factors might be the sources of improved magnetic properties.

In this work, a sol–gel auto-combustion method was employed to synthesize Sr-doped bismuth ferrites with composition as $Bi_{1-x}Sr_xFeO_3$ (x=0.0, 0.05, 0.10, 0.20, and 0.30). This technique has emerged as a unique method to prepare the oxide materials in phase pure form. The structural, dielectric and ferromagnetic properties of samples were characterized [9,10]. The substitution of divalent Sr ion at trivalent Bi-sites might create charge imbalance and oxygen vacancies in doped samples. Additionally, the doping of Sr at Bi-site could compress the spins and break its antiferromagnetic behavior, due to greater ionic radius of Sr than that of Bi. This would induce magnetization in BFO [11–13].

2. Experimental procedures

Glycine was used as a fuel agent to prepare Sr-doped bismuth ferrite ($Bi_{1-x}Sr_xFeO_3$, x=0.0, 0.05, 0.10, 0.20 and 0.30) samples using sol–gel auto-combustion technique. All the reagents used, bismuth nitrate pentahydrate [$Bi(NO_3)_3 \cdot 5H_2O$, 99%, Sigma Aldrich], iron nitrate nonahydrate [$Fe(NO_3)_3 \cdot 9H_2O$, 99.9%, Merck], strontium nitrate [$Sr(NO_3)_2$, 99.9%, Merck] and nitric acid [HNO_3], were of analytical grade purity. Bismuth nitrate is less soluble in distilled water, so it is dissolved in 50 ml HNO_3 having molarity 3 M. The other reagents were dissolved in 100 ml deionized water. The solutions were mixed and appropriate quantity of glycine was added into the solution. The mixture was placed on a hot plate at 90 °C and stirred continuously using magnetic capsule till it became a dark viscous resin. When the gel was formed, the temperature was increased up to 400 °C and continuous heating led to auto-ignition of dried resin with the evolution of large quantity of gases. The brownish color ash obtained after combustion was analyzed for perovskite type $BiFeO_3$ phase. The whole process took about 4 h but the time of actual ignition was less than 20 s. The fine powder was sintered at 600 °C in a muffle furnace. The flow chat of preparation steps is shown in Fig. 1 [14]. The pellets were formed using a steel dye of 16 mm diameter, using an Apex hydraulic press. The pellets were sintered in air at 300 °C for 2 h in a muffle furnace. The crystal structure of the samples was determined using a Rigaku D/MAX-II A diffractometer with CuK_α radiations. Dielectric properties were evaluated using a 1920 LCR meter to check storage ability of material. A S-3700 N (Hitachi Japan) scanning electron microscope (SEM) equipped with an energy dispersive X-ray (EDX) system was employed for morphological and compositional analysis. A 7404-Lakeshore vibrating sample magnetometer (VSM) was used to obtain the hysteresis loops for the magnetic studies of samples.

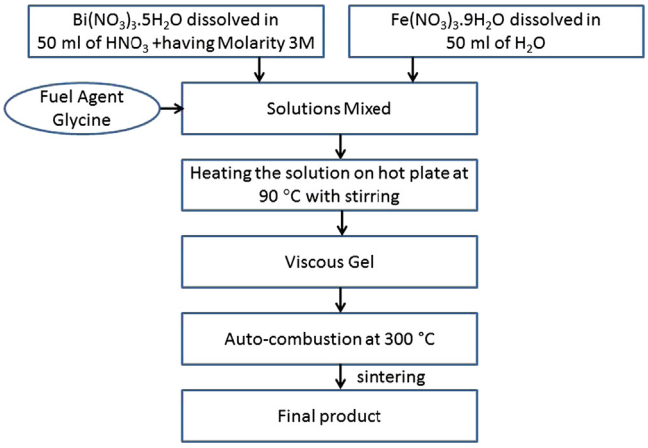

Fig. 1 The flow chat of preparation of $BiFeO_3$ by sol–gel auto-combustion process.

3. Results and discussion

The XRD patterns of all the prepared samples are shown in Fig. 2. The patterns indicate the formation of rhombohedral perovskite structure related to BFO, as all the major peaks were matched with the ICSD Reference no. 01-071-2494. Small impurity peak related to Bi_2O_3 (marked as ✻) and an unknown peak (marked as ●) were also identified in the un-doped sample. However, these impurity peaks were removed when the Sr concentration was increased in the series $Bi_{1-x}Sr_xFeO_3$, $x=0$, 0.05, 0.10, 0.20 and 0.30, but the peaks of secondary phase $Bi_2Fe_4O_9$ (marked as ◊) of bismuth ferrite were appeared. The intensities of these impurity peaks were increased as the Sr concentration was increased, depicting the limits of Sr doping in BFO [11,15].

The crystallite sizes of all the samples ($Bi_{1-x}Sr_xFeO_3$, $x=0.0$, 0.05, 0.10, 0.20, and 0.30) were obtained by considering the most intense diffraction peak in the pattern using Sherrer's formula [16], given as,

$$\text{Crystallite size} = 0.94\lambda/B\cos\theta \quad (1)$$

Here, 'λ' is the wavelength of the incident radiation, 'B' is the full width at half maximum in radians and 'θ' is the diffraction angle. The overall width of the most intense peaks of all samples was almost the same so the crystallite size of all samples remained nearly same having values in the range of 11.06 ± 0.001. The lattice parameters of unit cell were found, using 'CELL' software by putting the '2θ' values of all diffraction peaks and the subsequent unit cell volumes of $Bi_{1-x}Sr_xFeO_3$ samples were evaluated, as listed in Table 1. The results were well in agreement with some previous reports [11,16]. It is evident from the results that a very small doping of Sr ion in $Bi_{1-x}Sr_xFeO_3$ ($x=0.05$) decreases the lattice constant 'c' and a very small increment is observed in the lattice constant 'a' and cell volume of

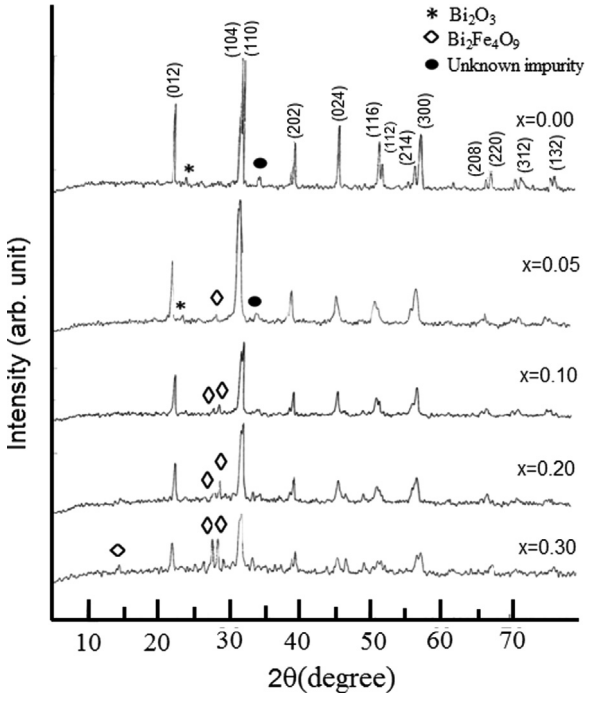

Fig. 2 XRD pattern of all the samples $Bi_{1-x}Sr_xFeO_3$ ($x=0.0$, 0.0.5, 0.10, 0.20, and 0.30).

Table 1 Unit cell parameters and volumes of all samples $Bi_{1-x}Sr_xFeO_3$ ($x=0.0$, 0.0.5, 0.10, 0.20, and 0.30).

Stoichiometry	a (Å)	c (Å)	V (Å^3)
$BiFeO_3$	5.5832	13.8684	374.4005
$Bi_{0.9}Sr_{0.05}FeO_3$	5.5840	13.7761	371.9989
$Bi_{0.90}Sr_{0.1}0FeO_3$	5.5856	13.7850	372.4638
$Bi_{0.80}Sr_{0.20}FeO_3$	5.5901	13.8014	373.5016
$Bi_{0.70}Sr_{0.30}FeO_3$	5.5959	13.8045	374.3602

$Bi_{0.95}Sr_{0.05}FeO_3$ sample becomes smaller than BFO. As the concentration of Sr ion increases from $x=0.05$, both the lattice parameters 'a' and 'c' increase gradually. The increment in 'c' in case of all other samples could be attributed to the formation of secondary phase of bismuth iron oxide $Bi_2Fe_4O_9$ [11,17].

The microstructural analysis of $Bi_{1-x}Sr_xFeO_3$ (for $x=0$, 0.10, 0.20 and 0.30) samples were carried out by using a JEOL SEM operated at 20 kV in its secondary image mode. The SEM micrographs of all the samples taken at a magnification of $\times$10,000 are shown in Fig. 3. The SEM image of pure BFO sample reveals grains with varying sizes but have well defined and sharp edges. The estimated grain sizes were evaluated in the range of 0.43–0.84 μm [18]. However, with Sr doping up to $x=0.10$, the morphology of grains changed completely as large sized grains were mainly vanished and small sized grains were dominant. The trend of decreasing grain size continued with increased Sr dopings ($x=0.20$ and 0.30). The micrographs of all the samples also revealed that the porosity of the samples decreased as the Sr doping was increased. The EDX spectra, revealing the presence of Bi, Sr, Fe, O and C contents, are in close agreement with the elemental composition of the dissolved reactants. Quantitative data of EDX analysis of $Bi_{1-x}Sr_xFeO_3$ ($x=0.0$, 0.10, 0.20 and 0.30) samples are provided in Table 2. Traces of carbon might be attributed to emerge from the sample stub [11,19].

Frequency dependent dielectric constant (ε') and dielectric loss factors (ε'') of $Bi_{1-x}Sr_xFeO_3$ ($x=0$, 0.05, 0.10, 0.20 and 0.30) samples were carried out by using a 1920 LCR meter manufactured by Quard Tech. The measurements were taken at RT (25 °C) in the frequency range of 100 Hz to 1 MHz and samples were used in disk form with approximate diameter of 16 mm and thickness of all the samples in range of 0.50–1.5 mm. ε' and ε'' measurements of all the samples were evaluated using the relation [11],

$$\varepsilon' = tC_p/A\varepsilon_0 = tC_p/\pi(d/2)^2\varepsilon_0 \quad (2)$$

where 't' is the thickness of pellet, 'C_p' is the equivalent parallel capacitance obtained experimentally, 'ε_0' is the permittivity of free space and 'd' is the diameter of the electrodes. 'ε''' is obtained from the measured value of dissipation factor. Here dissipation factor and equivalent parallel capacitance is obtained directly from the measurements [20]. It is observed that ε' is decreased rapidly by increasing frequency and becomes independent at high frequencies. The decrement in ε' is attributed to the dielectric relaxation. The dielectric dispersion can be explained by Koop's theory. According to this theory, the dielectric structure was imagined to consist of double layers. One layer is conducting and other layer is insulating. According to structural point of view, dielectric relaxation is directly related to orientational polarization [20,21]. When external electric field is applied, the atoms of the dielectric material takes some time to align them in the direction of electric field and that time is called relaxation time which is mostly

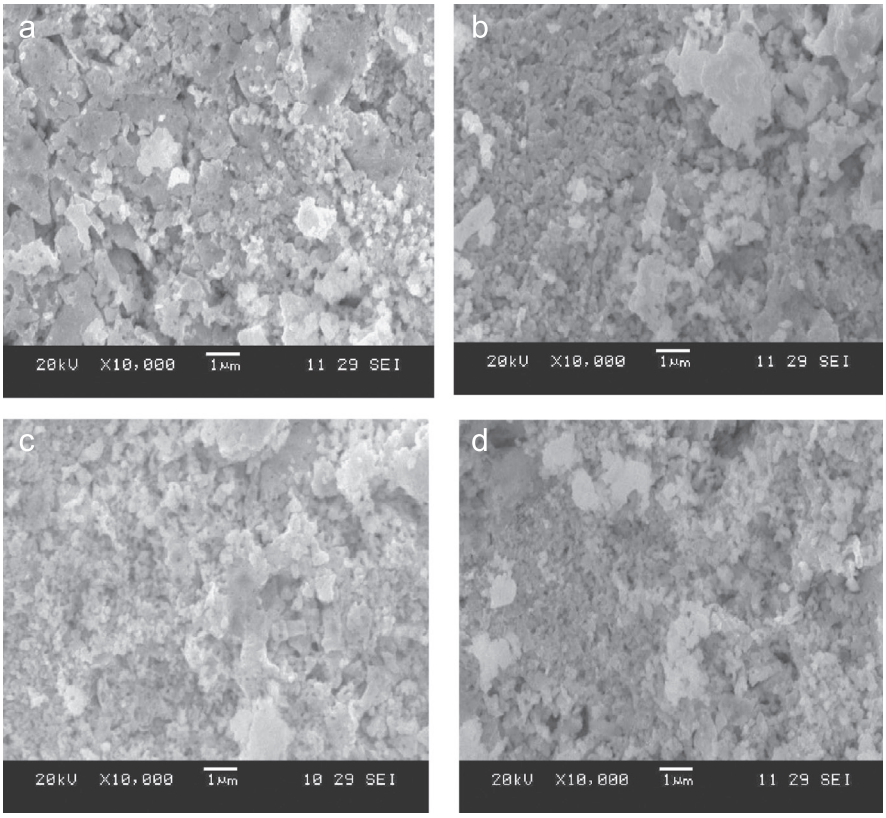

Fig. 3 SEM images of all samples of $Bi_{1-x}Sr_xFeO_3$: (a) $x=0.00$, (b) $x=0.10$, (c)$=0.20$ and (d) $x=0.30$.

Table 2 Quantities data of EDX of all the samples $Bi_{1-x}Sr_xFeO_3$ ($x=0.0$, 0.10, 0.20, and 0.30).

Elements	$BiFeO_3$		$Bi_{0.90}Sr_{0.10}FeO_3$		$Bi_{0.80}Sr_{0.20}FeO_3$		$Bi_{0.70}Sr_{0.30}FeO_3$	
	wt%	at%	wt%	at%	wt%	at%	wt%	at%
Bi	65.88	18.73	61.53	17.52	57.70	16.23	52.80	14.21
Sr	–	–	2.80	2.12	6.01	3.85	9.26	5.89
Fe	17.01	18.98	19.23	19.26	19.31	19.38	19.32	19.41
O	15.91	58.46	15.25	58.40	15.82	58.49	17.48	59.31
C	1.20	3.87	1.19	2.70	1.16	2.05	1.14	1.18

equal to 10^{-9} s [22]. It is observed that the decrement in ε' with increasing frequency is assigned to the fact that atoms in the dielectric material need a finite time to align up their axis in the applied electric field direction. As the frequency of the electric field increases, a point is reached when charge carriers of dielectric do not align with applied electric field so polarization cannot reach at its saturation point and do not follow the alteration of electric field. Hence, the value of ε' is decreased. When the frequency of the field continues to increase, at last, the polarization would hardly have started to move before the field reverses and makes no contribution to polarization and so ε' becomes independent at high frequencies. Another very important point of the decrement in dielectric constant is related with the hopping of electrons from Fe^{2+} to Fe^{3+} ions as these electrons require large amount of energy. At low frequency, electric field does not provide enough energy to electron for hopping but as we increase the frequency of electric field then it provides sufficient energy and a point is reached when hopping of electron is started from Fe^{2+} to Fe^{3+}. That is why conductivity of the dielectric increases as frequency is increased and hence a decrement occurs in ε' [22]. The frequency–dielectric constant relationship of all the samples is plotted in Fig. 4. The ε' value of pure BFO is observed as 52 at 100 Hz and it decreases with increase in frequency and becomes constant at high values of frequency. Further decrease in the value of ε' was observed as Sr was doped at Bi-sites. This behavior could be attributed to the increase of conductivity in the Sr-doped samples [23,24]. When the relaxation time of dielectric material and the frequency of the applied field become similar, a phase lag occurs and energy observed in dielectric material is called dielectric loss which can be calculated by a relation,

$$\text{Tan}\,\theta = \varepsilon''/\varepsilon' \tag{3}$$

The behavior of ε'' is similar to the ε'. The dielectric loss of all samples $Bi_{1-x}Sr_xFeO_3$ ($x=0.0$, 0.05, 0.10, 0.20 and 0.30) decreases with increasing frequency. The dielectric loss means loss of energy in dielectric material [19–23]. The trend of the

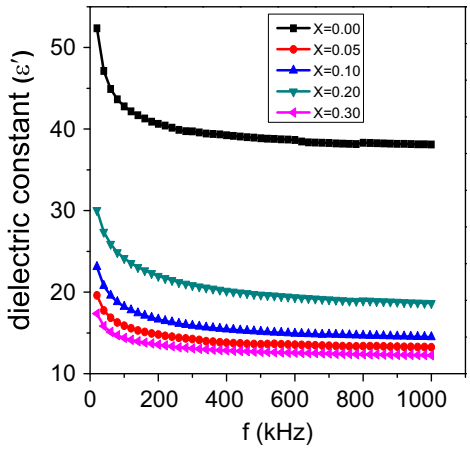

Fig. 4 Dependence of dielectric constant on frequency of all samples $Bi_{1-x}Sr_xFeO_3$ (x=0.0, 0.05, 0.10, 0.20, and 0.30).

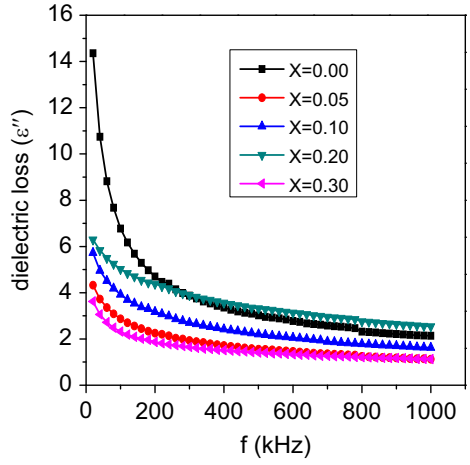

Fig. 5 Dependence of dielectric loss (ε'') on frequency of all the samples $Bi_{1-x}Sr_xFeO_3$ (x=0.0, 0.05, 0.10, 0.20, and 0.30).

dielectric loss as a function of Sr doping in the series of samples is shown in Fig. 5.

Temperature dependent ε' and ε'' measurements of all the samples $Bi_{1-x}Sr_xFeO_3$ (x=0.0, 0.050, 0.10, 0.20 and 0.30) were carried out in temperature range 40–200 °C at a fixed frequency 20 kHz. ε' of most of the magnetic materials increases with increasing temperature [25]. In pure BFO, ε' decreases up to 100 °C in very small value. Then upon further heating, it is increased. The Sr-doped samples showed a minute increase in the ε', as shown in Fig. 6.

The ε'' factor of the samples $Bi_{1-x}Sr_xFeO_3$ (x=0.0, 0.10 and 0.30) was also determined in the temperature range of 40–200 °C and was found to increase by increasing the temperature. This is due to the fact that by increasing temperature, the resistance of dielectric material is increased and more energy is dissipated in dielectric material [25]. The relation between dielectric loss and temperature of the samples $Bi_{1-x}Sr_xFeO_3$ (x=0.0, 0.10 and 0.30) is shown in Fig. 7.

The magnetic hysteresis (M–H) loops of all the samples have been provided in Fig. 8. The loops reveal that the saturation magnetization (M_s) of all samples is achieved below 1000 Oe. The magnetization of pure BFO increases almost linearly with applied magnetic field and no spontaneous magnetization is evident from the M–H loop of the sample. In addition, nearly zero remanent magnetization (M_r)

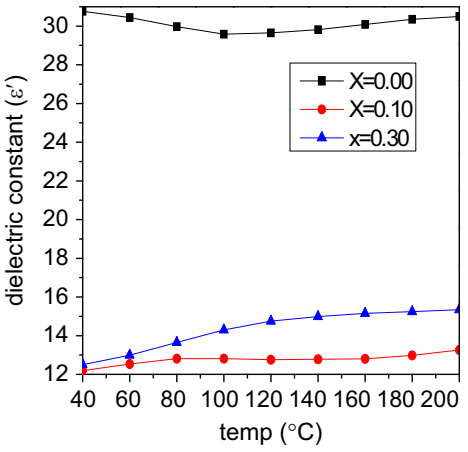

Fig. 6 Dependence of dielectric constant on temperature of $Bi_{1-x}Sr_xFeO_3$ (x=0.0, 0.10, and 0.30).

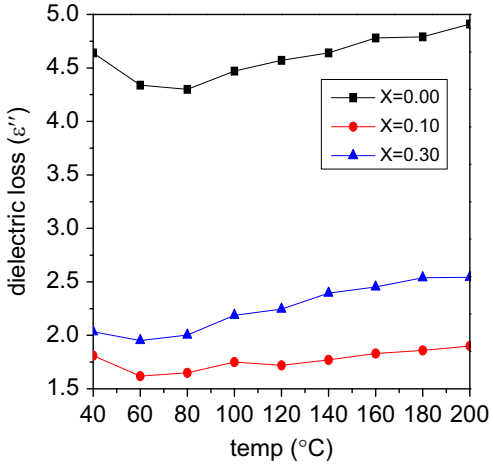

Fig. 7 Dependence of dielectric loss on temperature of $Bi_{1-x}Sr_xFeO_3$ (x=0.0, 0.10, and 0.30).

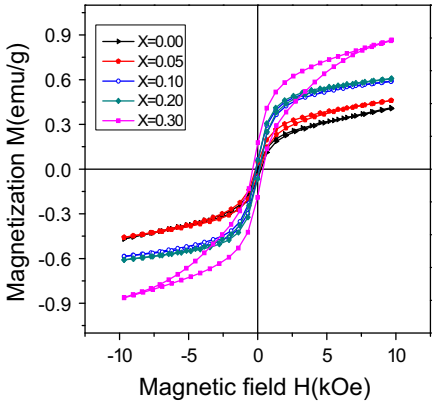

Fig. 8 M–H loops of $Bi_{1-x}Sr_xFeO_3$ (x=0.00, 0.05, 0.10, 0.20, and 0.30) samples.

is observed and hence confirming the antiferromagnetic nature of the $BiFeO_3$ sample [7]. The results show that by increasing the concentration of divalent Sr^{2+} ions at Bi-site in BFO, the fraction of Fe^{3+} ions change into Fe^{4+} ions. This substitution favours a possibility of

presence of some oxygen vacancies in order to compensate the charge of doped BFO samples. The Mössbauer spectroscopy of Sr-doped BFO material has not supported the formation of Fe^{4+} or Fe^{2+} ions in doped BFO material [11]. Therefore, it is understood that oxygen vacancies must have been created in material to compensate the charge imbalance which is created by doping of Sr^{2+} ions in place of Bi^{3+} ions. In pure BFO, Fe^{3+}–O–Fe^{3+} chains show antiferromagnetic behavior [26]. The oxygen vacancies increase the bond angle of Fe^{3+}–O–Fe^{3+} and the spin of Fe^{3+} ions are canted and net magnetization is induced. The value of magnetization increases with increasing doping concentration of Sr^{2+} ions, as with enhanced Sr^{2+} doping, more oxygen vacancies are created and the bond angle of Fe^{3+}–O–Fe^{3+} continues to increase. Hence, more spins are canted which subsequently enhance the magnetization [11,26]. Oxygen vacancies are not the only factor to enhance the net magnetization of $Bi_{1-x}Sr_xFeO_3$ ($x=0.0$, 0.05, 0.10, 0.20 and 0.30) series. Ionic radii of the doped element could also play an important role to enhance the magnetization of $BiFeO_3$. The ionic radii of doping element must be greater than Bi^{3+} ionic radii. The greater ionic radii of the doped element, suppresses the spiral spin structure and the inversion symmetry is broken [27]. The structure is changed into cycloidal type structure and net magnetization is induced in doped $BiFeO_3$ material. It is evident from Fig. 8 that the magnetization increases linearly by applying magnetic field and no remanent magnetization is present in pure BFO sample [11,27]. The maximum values of saturation magnetization, remanence and coercivity were achieved as 0.867 emu/g, 0.175 emu/g and 366.64 Oe, respectively for a Sr doping of $x=0.30$.

4. Conclusions

$BiFeO_3$ was successfully synthesized using sol–gel auto-combustion technique. However, a secondary phase ($Bi_2Fe_4O_9$) of bismuth ferrite was detected in all Sr-doped samples. Lattice parameters were changed with the substitution of Sr at Bi-site. The crystallite size remained almost invariable with the substitution of Sr. The structural morphology of the samples determined using SEM exhibited that the grain size was reduced as the Sr-contents were increased in $BiFeO_3$. The dielectric constant of pure $BiFeO_3$ was found 52 at 100 Hz frequency and decreased with increasing frequency and became constant at high frequency. It also decreased with increasing Sr concentration and the lowest value of 17.4 at 100 Hz was noticed at $x=0.30$. The value of dielectric loss also displayed the same behavior. The values of dielectric constant and dielectric loss factor were observed to increase slightly in the Sr-doped sample as the temperature was increased up to 200 °C. Saturation magnetization and coercivity were found to increase as the Sr-contents were increased and found as 0.867 emu/g and 336.64 Oe, respectively, for Sr contents of $x=0.30$.

Acknowledgment

First author would like to thank Shahzad Naseem, Saira Riaz and M. Sabieh Anwar for their help in some experimental measurements.

References

[1] C. Binek, X. He, Y. Wang, S. Sahoo, Christian Binek Publications, vol. 65, 2008, pp. 1–9.
[2] Q. He, Y.H. Chu, J.T. Heron, S.Y. Yang, W.I. Liang, C.Y. Kuo, H.J. Lin, P. Yu, C.W. Liang, R.J. Zeches, W.C. Kuo, J.Y. Juang, C.T. Chen, E. Arenholz, A. Scholl, R. Ramesh, Nature Communications 2 (2011) 225–229.
[3] W. Eerenstein, N.D. Mathur, J.F. Scott, Nature 442 (2007) 759–765.
[4] D. Khomskii, Physics 2 (2009) 20–27.
[5] V.B. Naik, R. Mahendiran, Solid State Communications 149 (2009) 754–758.
[6] P. Ravindran, R. Vidya, A. Kjekshus, H. Fjellvag, Physical Review B 74 (2006) 224412–224429.
[7] V.A. Khomchenko, D.A. Kiselev, M. Kopcewicz, M. Maglione, V.V. Shvartsman, P. Borisov, W. Kleemann, A.M.L. Lopese, Y.G. Pogorelov, J.P. Araujo, R.M. Rubinger, N.A. Sobolev, J.M. Vieira, A.L. Kholkin, Journal of Magnetism and Magnetic Materials 321 (2009) 1692–1698.
[8] J.K. Kim, S.S. Kim, W.J. Kim, Materials Letters 59 (2005) 4006–4009.
[9] G.S. Lotey, N.K. Verma, Journal of Nanoparticle Research 14 (2012) 742–752.
[10] J. Wei, D. Xue, Materials Research Bulletin 43 (2008) 3368–3373.
[11] B. Bhushan, A. Basumallick, N.Y. Vasanthacharya, S. Kumar, D. Das, Solid State Sciences 12 (2010) 1063–1069.
[12] P. Singh, Y.A. Park, K.D. Sung, N. Hur, J.H. Jung, W.S. Noh, J.Y. Kim, J. Yoon, Y. Jo, Solid State Communications 150 (2010) 431–434.
[13] A. Moure, J. Tartaj, C. Moure, Journal of Alloys and Compounds 509 (2011) 7042–7046.
[14] S. Farhadi, M. Zaidi, Journal of Molecular Catalysis A: Chemical 299 (2009) 18–25.
[15] L.Y. Wang, D.H. Wang, H.B. Huang, Z.D. Han, Q.Q. Cao, B.X. Gu, Y.W. Du, Journal of Alloys and Compounds 469 (2009) 1–3.
[16] C. Fu, M. Huo, W. Cai, X. Deng, Journal of Ceramic Processing Research 13 (2012) 561–564.
[17] G. Ali, S.A. Siddiqi, S.M. Ramay, S. Atiq, M. Saleem, International Journal of Minerals, Metallurgy and Materials 20 (2013) 166–171.
[18] Z. Dai, Y. Akishige, Journal of Physics D: Applied Physics 43 (2010) 445403–445407.
[19] X. Yu, X. An, Solid State Communications 149 (2009) 711–714.
[20] E. Markiewicz, B. Hilczer, M. Błaszyk, A. Pietraszko, E. Talik, Journal of Electroceramics 27 (2011) 154–161.
[21] S.R. Shannigrahi, A. Huang, N. Chandrasekhar, D. Tripathy, A.O. Adeyeye, Applied Physics Letters 90 (2007) 022901–022903.
[22] Y.K. Jun, W.T. Moon, C.M. Chang, H.S. Kim, H.S. Ryu, J.W. Kim, K.H. Kim, S.H. Hong, Solid State Communications 135 (2005) 133–137.
[23] A. Gautam, V.S. Rangra, Crystal Research and Technology 45 (2010) 953–956.
[24] P. Singh, K.D. Sung, Y.A. Park, N. Hur, J.H. Jung, Journal of the Korean Physical Society 55 (2009) 609–612.
[25] A.Y. Kim, S.H. Han, H.W. Kang, H.G. Lee, J.S. Kim, C.I. Cheon, Ceramics International 38 (2012) 397–401.
[26] C. Yang, J.S. Jiang, F.Z. Qian, D.M. Jiang, C.M. Wang, W.G. Zhang, Journal of Alloys and Compounds 507 (2010) 29–32.
[27] P. Singh, J.H. Jung, Physica B 405 (2010) 1086–1089.